Journal of The Electrochemical Society, **157** (6) H666-H670 (2010)
0013-4651/2010/157(6)/H666/5/$28.00 © The Electrochemical Society

Low Resistance Ohmic Contacts to Bi_2Te_3 Using Ni and Co Metallization

Rahul P. Gupta,[a,z] K. Xiong,[a] J. B. White,[b] Kyeongjae Cho,[a,*] H. N. Alshareef,[c] and B. E. Gnade[a,z]

[a]*Department of Materials Science and Engineering, University of Texas at Dallas, Richardson, Texas 75080, USA*
[b]*Marlow Industries Incorporated, a subsidiary of II-VI Incorporated, Dallas, Texas 75238, USA*
[c]*Materials Science and Engineering, King Abdullah University of Science and Technology, Thuwal 23955-6900, Saudi Arabia*

A detailed study of the impact of surface preparation and postdeposition annealing on contact resistivity for sputtered Ni and Co contacts to thin-film Bi_2Te_3 is presented. The specific contact resistivity is obtained using the transfer length method. It is observed that in situ sputter cleaning using Ar bombardment before metal deposition gives a surface free of oxides and other contaminants. This surface treatment reduces the contact resistivity by more than 10 times for both Ni and Co contacts. Postdeposition annealing at 100°C on samples that were sputter-cleaned further reduces the contact resistivity to $<10^{-7}$ Ω cm^2 for both Ni and Co contacts to Bi_2Te_3. Co as a suitable contact metal to Bi_2Te_3 is reported. Co provided similar contact resistance values as Ni, but had better adhesion and less diffusion into the thermoelectric material, making it a suitable candidate for contact metallization to Bi_2Te_3 based devices.
 [DOI: 10.1149/1.3385154]

Manuscript submitted December 10, 2009; revised manuscript received March 15, 2010. Published April 27, 2010.

Thermoelectric (TE) coolers have been extensively used in the optoelectronic, automotive, space, and semiconductor industries where low device operational temperature is key to device performance in terms of speed and reliability.[1-3] However, despite these advantages the use of TE devices has been limited for high watt density applications.[4] To allow TE coolers to reach the next level in terms of performance and power density, the thickness of the device needs to be scaled down.[5] Contact resistance becomes a serious limitation to the efficiency of TE material based solid-state coolers with thermoelement leg lengths <100 μm, as can be seen in Fig. 1, where the ratio of device figure-of-merit (Z_d) and material figure-of-merit (Z_m) is plotted vs the thermoelement leg length (L) as a function of contact resistance.[6] The relationship between Z_d and Z_m is given by Eq. 1 [7]

$$Z_d = Z_m\left[\frac{L}{L + 2r_c\sigma}\right] \quad [1]$$

where L is the thermoelement leg length, r_c is the contact resistance, and σ is the bulk conductivity.

As can been seen in Fig. 1a, for a device leg length of 100 μm, Z_d/Z_m drops from 0.9 to 0.5 as the contact resistivity increases from 5×10^{-7} to 5×10^{-6} Ω cm^2. The resulting drop in the device dimensionless figure-of-merit Z_dT impacts the coefficient of performance (COP) of the device as shown in Fig. 1b, which can be expressed as[8]

$$\mathrm{COP}_{max} = \frac{T_c}{T_h - T_c} \times \frac{\sqrt{1 + \frac{Z(T_c + T_h)}{2}} - \frac{T_h}{T_c}}{\sqrt{1 + \frac{Z(T_c + T_h)}{2}} + 1} \quad [2]$$

where T_c and T_h represent the temperature of the cold side and the hot side, respectively. Therefore, from a device point of view, although a high Z material can be achieved, the device COP can still be low due to the degradation of Z due to the contact resistivity. For thin TE materials, the losses become even more extreme and low electrical contact resistivity of $<10^{-7}$ Ω cm^2 is needed to minimize the impact of contact resistance on COP. High contact resistance at the electrode/TE material interface remains a challenge that is limiting widespread adoption of TE technology in many applications.

For industry standard TE devices, electroless plated Ni is used as a diffusion barrier to Cu and solder components such as Sn. However, electroless Ni gives a relatively high contact resistivity ($>5 \times 10^{-6}$ Ω cm^2).[9] Bi_2Te_3 is a small bandgap semiconductor with a bandgap of 0.16 eV. Therefore it is theoretically possible to obtain a very low contact resistance, $<10^{-7}$ Ω cm^2, for an ideal metal–semiconductor contact; however, real metal–semiconductor interfaces are far more complex.[10] Extrinsic factors such as unwanted impurities and structural imperfections tend to accumulate at the interface and dominate the behavior of the metal–semiconductor interface.[11] The optimization of processing methods such as surface preparation, cleaning, metal deposition, and alloying for the fabrication of practical metal–semiconductor contacts becomes important to achieve a near ideal contact.[12] A detailed study of the effect of surface preparation and heat-treatment on contact resistance for sputtered Ni contacts to thin-film Bi_2Te_3 is presented. The contact resistance values obtained using the transfer length method (TLM) for Ni are compared to Co as a potential contact metal to Bi_2Te_3.

Experimental

Thermal SiO_2 (100 nm) on Si was used as the insulating layer for Bi_2Te_3 mesa isolation. A lift-off process was used to define the mesa pattern (layer 1) using a standard photolithography process. After patterning layer 1 using photoresist S1813, 5 nm of Cr was E-beam evaporated as an adhesion layer between the Bi_2Te_3 and the SiO_2. Bi (100 nm) and Te (142 nm) were deposited as a bilayer on the substrate using E-beam evaporation. The thickness of Bi and Te was carefully chosen so that a stoichiometric film of Bi_2Te_3 was produced. After lift-off and visual inspection, the sample was annealed at 200°C for 2 h under vacuum at 10^{-7} Torr. For a qualitative assessment of the Bi_2Te_3 films, grazing incidence X-ray diffraction (GIXRD) was used for the structural characterization of the as-deposited and annealed Bi_2Te_3 films using a Rigaku ULTIMA III system with Cu Kα (λ = 1.54 Å) X-ray radiation, operated at 40 kV and 44 mA. Surface analysis to compare different cleaning methods was done using monochromatic X-ray photoelectron spectroscopy (XPS) using an Al K (1486.7 eV) X-ray source with a linewidth of ~0.25 eV and pass energy of 15 eV. Due to the difficulty in finding etchants which preferentially etch metals such as Ni and Co, but stop on Bi_2Te_3, layer 2 was patterned using lift-off. Figure 2a and b shows the schematic cross-sectional view of the layers and a top view of an actual sample after fabrication. An AJA ATC Orion 4 HV magnetron system was used to sputter Ni and Co onto the patterned samples. The Co and Ni films were deposited for 30 min at

* Electrochemical Society Active Member.
z E-mail: rahul.utd@gmail.com; gnade@utdallas.edu

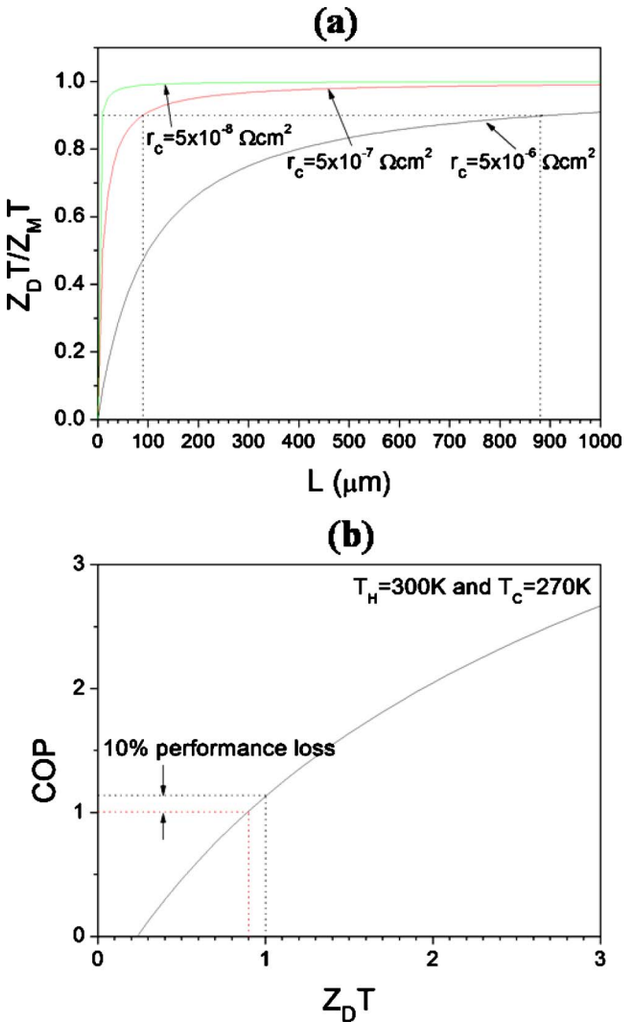

Figure 1. (Color online) (a) Ratio of device figure-of-merit (Z_d) to material figure-of-merit (Z_m) is plotted against TE leg length (L), and (b) COP is plotted against device figure-of-merit (Z_d)

9 and 8 nm/min, respectively, at room temperature at a pressure of 4 mTorr and a power density of 10 W/cm^2 using Ar as the sputter gas. Table I summarizes the set of samples prepared to compare the impact of surface preparation, postannealing, and metals on the contact resistance. The solvent-cleaned samples were rinsed with acetone, isopropyl alcohol (IPA), and deionized (DI) water before

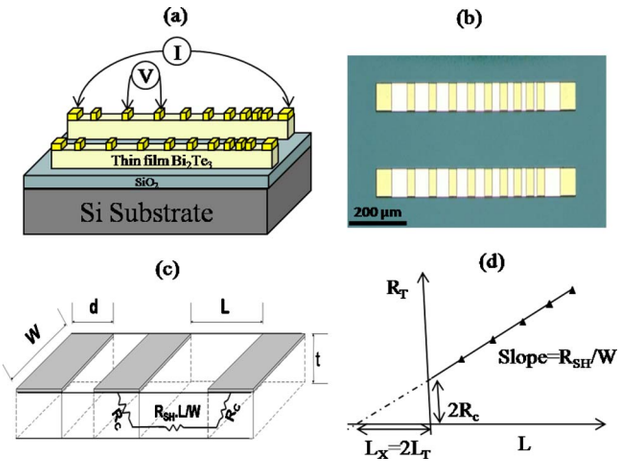

Figure 2. (Color online) (a) Schematic cross section of the layers after patterning. (b) Optical micrograph showing top view of actual sample after fabrication. (c) A general schematic of a TLM structure. (d) An example of the total resistance (R_t) vs pad distance (L) plot to extract R_c, R_{sh}, and L_t.

loading in the deposition system. The samples that were in situ Ar^+ sputtered just before the metal deposition were bombarded with Ar^+ ions at 50 W at a pressure of 10 mTorr for 10 min. The postannealing was done at different temperatures (100 and 200°C) for 2 h at a pressure of 10^{-7} Torr.

Contact Resistance Measurement

The two terminal multiple contact resistor method originally proposed by Shockley,[13] also known as the TLM, was used to measure contact resistance (R_c) and to extract the contact area-independent term specific contact resistivity (ρ_c).[14] Separate metal pads on each side of the mesa, as can be seen in Fig. 2, were designed for uniform current flow under the contacts.[15] The total resistance measured between adjacent metal pads is given by[16]

$$R_t = \frac{R_{sh}}{W}L + \frac{2L_tR_{sk}}{W} \quad [3]$$

where R_t is the total measured resistance, R_{sh} is the Bi_2Te_3 sheet resistance, R_{sk} is the modified sheet resistance under the contact, L_t is the transfer length, W is the contact width, and L the distance between the adjacent metal pads. Contact resistance, R_c is given by

$$R_c = \frac{L_tR_{sk}}{W} \quad [4]$$

The total resistance is measured between each set of pads and plotted vs the pad spacing. Using Eq. 3 and 4, the contact resistance

Table I. Sample identification for samples used in this study and summary of the specific contact resistivities and the bulk resistivities extracted from TLM measurements.

Sample identification	Sputtered metal	Surface treatment	Postannealing (°C)	Specific contact resistivity (μΩ cm^2)	Bulk resistivity (mΩ cm)
Ni_S	Ni	Solvent-cleaned	None	189.51 ± 40.08	4.94
Ni_S_100	Ni	Solvent-cleaned	100	797.03 ± 70.45	3.54
Ni_Ar	Ni	Solvent-cleaned + Ar sputter-cleaned	None	1.49 ± 0.32	2.66
Ni_Ar_100	Ni	Solvent-cleaned + Ar sputter-cleaned	100	0.07 ± 0.03	2.47
Ni_Ar_200	Ni	Solvent-cleaned + Ar sputter-cleaned	200	<0.01	1.84
Co_S	Co	Solvent-cleaned	None	13.22 ± 1.69	4.22
Co_S_100	Co	Solvent-cleaned	100	11.35 ± 5.99	3.73
Co_Ar	Co	Solvent-cleaned + Ar sputter-cleaned	None	2.08 ± 0.78	2.47
Co_Ar_100	Co	Solvent-cleaned + Ar sputter-cleaned	100	0.04 ± 0.03	2.29
Co_Ar_200	Co	Solvent-cleaned + Ar sputter-cleaned	200	<0.01	3.21

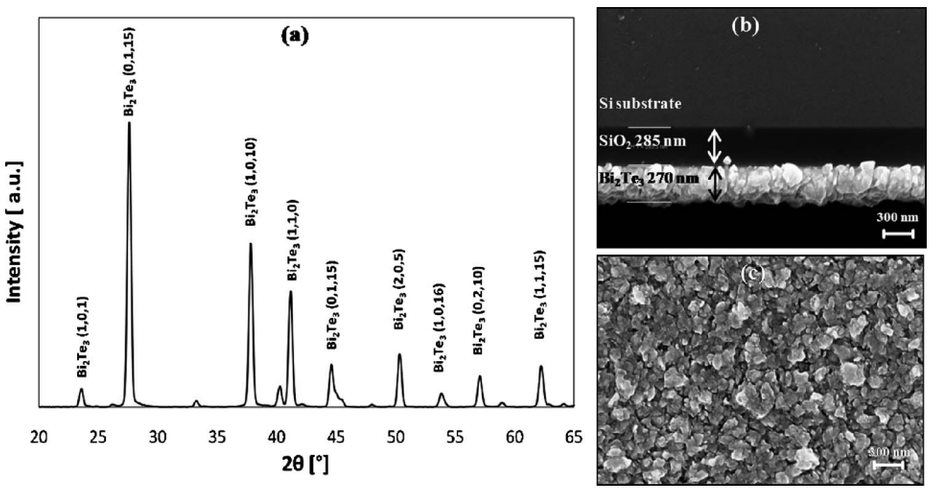

Figure 3. (a) Thin-film GIXRD curve for Bi–Te showing Bi_2Te_3 phase formation. All the peaks are consistent with polycrystalline Bi_2Te_3. (b) Cross-sectional SEM micrograph of postannealed Bi_2Te_3 film. (c) SEM micrograph of surface morphology of Bi_2Te_3 film.

can be obtained from the *y*-intercept, $2R_c$, and the semiconductor sheet resistance from the slope, R_{sh}/W. From Eq. 3, the *x*-intercept, L_x, gives additional information about the transfer length, L_t, and the effective semiconductor sheet resistance, R_{sk}, under the pads. Lundberg and Östling[17] defined L_t as the distance from the edge of the contact at which the current has dropped to 1/e of its original value at the leading edge. The transfer length is related to the distance needed for the current to flow in or out of the contact. The effective sheet resistance is related to the change in the sheet resistance from alloying. If R_{sh} and R_{sk} are equal, then L_x is simply $2L_t$ and "$W \times L_t$" becomes the effective area; therefore

$$\rho_c = R_c W L_t \qquad [5]$$

For this work, we assume $R_{sh} = R_{sk}$, therefore using Eq. 5 for the specific contact resistivity calculation.

As shown in Fig. 2a, the TLM structures consist of a thin-film Bi_2Te_3 mesa (100×1300 μm) with several metal pads (100×50 μm) separated by 10, 20, 30, 40, 50, 60, 70, 80, and 90 μm. A four-point probe method that reduces parasitic effects such as probe resistance and probe contact resistance was used to measure the total resistance. Force probes (I) were placed on metal pads (100×100 μm) on each end of the mesa and the sense probes (V) were placed on top of the metal pads that were being measured. Resistance measurements were taken at a fixed current of 1 mA (averaged over 10 points). The voltage difference was measured for the adjacent metal pads. The data were recorded using an LR2000 Quadtech milliohm meter. The total resistance was plotted vs the pad separation, as shown in Fig. 2d.

Results and Discussion

X-ray diffraction (XRD) data of postannealed Bi_2Te_3 thin films formed using sequential evaporation of Bi and Te show that Bi_2Te_3 is the only phase present, as shown in Fig. 3a. Other compound phases of Bi–Te were either not present or were present below the detection limit of GIXRD. Figure 3b shows a cross-sectional scanning electron microscopy (SEM) micrograph of the postannealed Bi_2Te_3 film, while Fig. 3c shows the surface morphology. It is observed that Bi and Te reacted completely to form polycrystalline Bi_2Te_3. Thin-film formation of Bi_2Te_3 using sequential evaporation of Bi and Te and postannealing was reported by Liao et al., but the annealing time has been considerably reduced in our case.[18,19]

Table I is a summary of all the samples tested in this study, the process conditions used, and the specific contact resistivity which was extracted. As a preliminary test, the ohmic vs Schottky nature of the contacts was tested. Linear current–voltage (*I-V*) curves were obtained, as shown in Fig. 4, for all the samples, indicative of ohmic contact formation. The total current is limited by the sum of the contact resistance plus the semiconductor resistance, so even though the current is less for the Co contacts, the contact resistance for Co and Ni are similar. Figures 5 and 6 show total resistance plotted as a function of pad spacing for Ni and Co contacts on thin-film Bi_2Te_3 for the TLM measurements. Figure 7 is a summary of the specific contact resistivities extracted from the TLM measurements for all the samples. Ni and Co show a reduction in contact resistivity by >10 times when the surface is in situ sputter-cleaned using Ar ion bombardment, as compared to solvent cleaning only. The contact resistivity for the Ni solvent-cleaned-only sample is reduced from 1.9×10^{-4} to 1.5×10^{-6} Ω cm^2 when Ar^+ sputter cleaning is added. The contact resistivity for the Co contacts is reduced from 1.3×10^{-5} to 2.1×10^{-6} Ω cm^2 when the Bi_2Te_3 substrate is sputter-cleaned. The reduction in the contact resistivity is attributed to the removal of oxides and other contaminants present on the Bi_2Te_3 surface. Figure 8a and b shows data for the Bi and Te photoelectron peaks comparing different surface cleaning methods. Sample A is as-grown with no surface cleaning; sample B is solvent-cleaned by rinsing with acetone, IPA, and DI water; sample C is solvent-cleaned followed by etching in 1:10 HNO_3:DI water for 60 s, followed by 20% Br_2 in methanol for 60 s and rinsing in DI water; and sample D is solvent-cleaned followed by in situ ion bombardment using Ar^+ ions at 50 W, 10 mTorr for 10 min before sputter deposition. Sample C shows partial removal of the surface oxides,

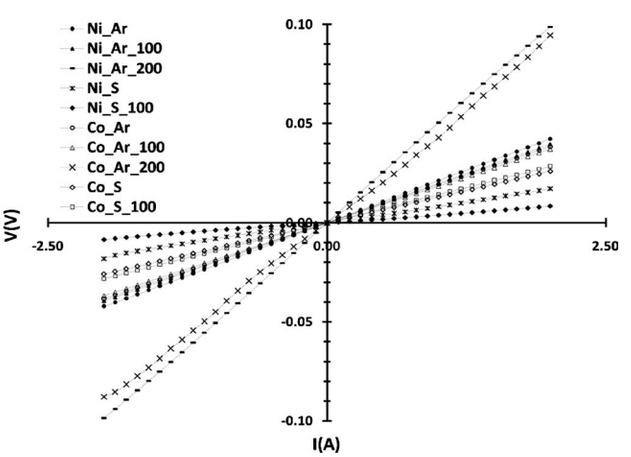

Figure 4. *I-V* characteristics for Ni and Co contacts measured between TLM pads with a spacing of 30 μm for different processing conditions. Solid filled markers indicate Ni while unfilled represent Co.

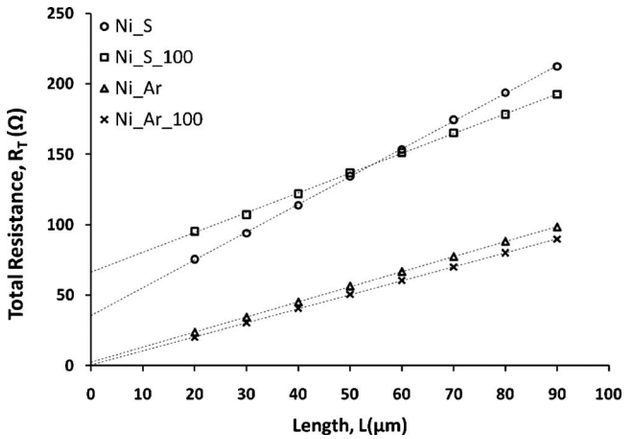

Figure 5. Total resistance is plotted as a function of pad spacing for Ni contacts on thin-film Bi_2Te_3 for TLM measurements. Sample processed at different postanneals and surface treatments are compared. Details of the process used for different samples are shown in Table I.

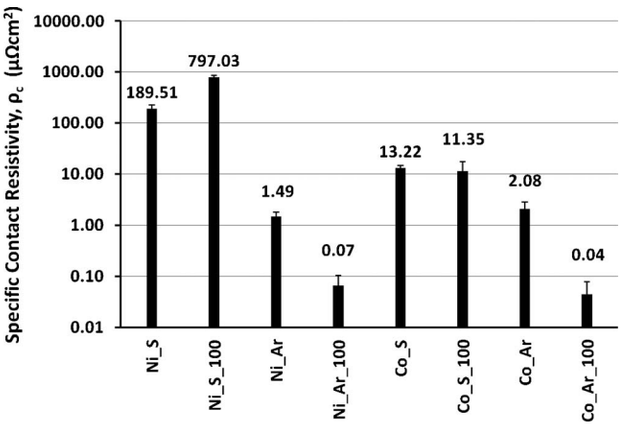

Figure 7. Summary of the specific contact resistivities extracted from TLM measurements.

but the complete removal of the native oxide was only possible using 10 min in situ Ar^+ sputter cleaning. The solvent-cleaned sample shows significant amounts of Bi and Te oxides at the surface, which is the reason for a higher contact resistivity.

As shown in Fig. 7, further reduction in the contact resistivity is achieved by postdeposition annealing at 100°C for Ar^+ sputter-cleaned samples. The specific contact resistivity is reduced by >10 times from 1.49×10^{-6} to 7×10^{-8} Ω cm² and from 2.08 $\times 10^{-6}$ to 4×10^{-8} Ω cm² for the Ni and Co contacts, respectively. As the measured specific contact resistivity is reduced the systematic measurement error becomes large. Ueng et al.,[20] reported that the contribution from systematic errors can become as much as ~106% for the specific contact resistivity $<10^{-7}$ Ω cm² for non-optimized TLM structures. The variation in the measured specific contact resistivity due to the systematic error plus random error was 55 and 76% for the Ni and Co contacts for 100°C postannealed samples, respectively. The overall reduction in the contact resistivity is much greater than the measurement error, indicating a significant improvement using the proposed process. The reductions in the contact resistivity at annealing temperatures as low as 100°C are attributed to the electrically favorable interfacial phase formation for both Ni and Co. Previous work on interfacial reactions[21] has shown the formation of NiTe and $CoTe_2$ as the preferred phases formed at temperature as low as 100°C for Ni and Co.

Calculations show that a reduction in the *y*-intercept from 5.5 to 1.8 Ω results in a reduction in the specific contact resistivity from 9.9×10^{-6} to 1×10^{-6} Ω cm², if the sheet resistance is held constant. A reduction from 0.2 to 0.1 Ω reduces the specific contact resistivity from 1×10^{-8} to 3×10^{-9} Ω cm². The specific contact resistivity is reduced by almost 10 times for just a 0.1 Ω change in the *y*-intercept for very low resistance contacts (~10^{-8} Ω cm²). The error from the measurement setup was measured to be ~1.1%, which generates more than ±0.1 Ω variations in the *y*-intercept. Therefore measurement of the specific contact resistivity $<10^{-8}$ Ω cm² is limited by our present experimental procedure.

The samples annealed at 200°C show a very high diffusivity for Ni.[22] The change in the sheet resistance due to significant alloying cannot be ignored for high temperature anneals. Effects such as change in the sheet resistance must be accounted for in the accurate measurement of contact resistivities $<10^{-8}$ Ω cm². The *I-V* curves for samples postannealed at 200°C show a lower total resistance and therefore the specific contact resistivity for the Ar^+ sputter-cleaned Ni and Co samples could be $<10^{-8}$ Ω cm², if the sheet resistance has not changed dramatically.

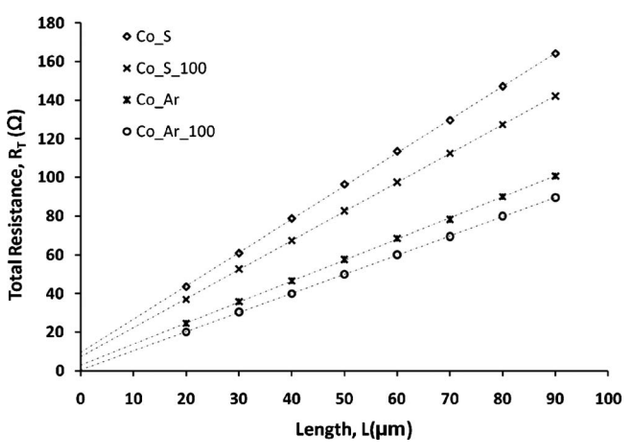

Figure 6. Total resistance is plotted as a function of pad spacing for Co contacts on thin-film Bi_2Te_3 for TLM measurements. Samples processed at different postanneals and surface treatments are compared. Details of the processes used for different samples are shown in Table I.

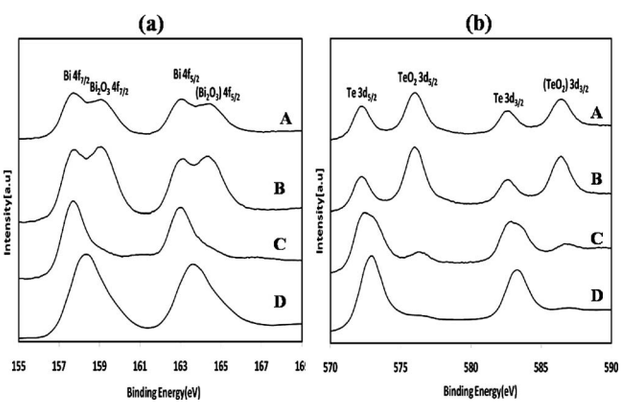

Figure 8. XPS spectra comparing different surface cleaning methods for (a) Bi and (b) Te region. Spectra labels for (a) and (b) are as follows, (A) not cleaned, (B) solvent-cleaned by rinsing with acetone, IPA, and DI water, (C) solvent-cleaned, dipped in 1:10 HNO_3:DI water solution for 60 s, followed by 20% Br_2 in Methanol for 60 s and rinsing in DI water, and (D) solvent-cleaned followed by ion bombardment using Ar^+ ions.

The electrical behavior for Co contacts is similar to Ni contacts even after postannealing. Results from previous work where first principle calculations were performed to study the stability of the interfaces, show the Co/Bi_2Te_3 interfaces to be more thermodynamically stable than the Ni/Bi_2Te_3 interfaces.[23] Co diffuses significantly less than Ni, therefore it is less likely to degrade the TE property of the TE material.[20] The film adhesion of Co deposited on Bi_2Te_3 at room temperature is better than Ni, based on adhesion test results using ASTM standard 3359-B. Therefore, Co contacts on thin-film Bi_2Te_3 postannealed at 100–200°C show potential advantages over Ni, both thermodynamically and mechanically, and are as good as Ni electrically.

Conclusions

We report improved contact resistivity values for contacts to thin-film Bi_2Te_3 by using the proper metal and surface engineering. The data indicate reduction in the contact resistivity by 10 times for metal–semiconductor interfaces free of oxides and other contaminants. A further reduction is attained with suitable alloying and phase formation by using low temperature postannealing. Specific contact resistivities $<10^{-7}$ Ω cm^2 were obtained for both Ni and Co contacts annealed at 100°C, when the substrates were in situ sputter-cleaned with Ar^+ ion bombardment. The specific contact resistivity for the postannealed samples at 200°C could not be accurately determined using our current TLM technique due to the magnitude of measurement errors generated for ultralow contact resistivity, but results suggest the contact resistivity is $<1 \times 10^{-8}$ Ω cm^2. Co contacts on thin-film Bi_2Te_3 postannealed at 100–200°C have advantages over Ni both thermodynamically and mechanically, and are as good as Ni electrically.

Acknowledgments

The authors thank the II-VI Foundation, a private foundation, for financial support of this work.

University of Texas at Dallas assisted in meeting the publication costs of this article.

References

1. V. Semenyuk, in *22nd International Conference on Thermoelectrics*, IEEE, p. 631 (2003).
2. S. B. Riffat, *Appl. Therm. Eng.*, **23**, 913 (2003).
3. J. Sharp, J. Bierschenk, and H. B. Lyon, *Proc. IEEE*, **94**, 1602 (2006).
4. D. T. Morelli, in *15th International Conference on Thermoelectrics*, IEEE, p. 383 (1996).
5. V. Semenyuk, in *20th International Conference on Thermoelectrics*, IEEE, p. 391 (2001).
6. L. Rushing, A. Shakouri, P. Abraham, and J. E. Bowers, in *16th International Conference on Thermoelectrics*, IEEE, p. 646 (1997).
7. L. I. Anatychuk and O. J. Luste, in *15th International Conference on Thermoelectrics*, IEEE, p. 279 (1996).
8. D. M. Rowe, *Thermoelectrics Handbook*, pp. 1–7, CRC Press, Boca Raton, FL (2006).
9. R. P. Gupta, J. B. White, O. D. Iyore, U. Chakrabarti, H. N. Alshareef, and B. E. Gnade, *Electrochem. Solid-State Lett.*, **12**, H302 (2009).
10. L. W. da Silva and M. Kaviny, *Int. J. Heat Mass Transfer*, **47**, 2417 (2004).
11. B. R. Gossick, *Surf. Sci.*, **21**, 123 (1970).
12. G. Y. Robinson, *Thin Solid Films*, **72**, 129 (1980).
13. W. Shockley, A. Goetzberger, and R. M. Scarlett, Report no. AFAL-TDR-64–207, AFA Lab, Wright-Patterson Air Force, OH (1964).
14. D. K. Schroder, *Semiconductor Material and Device Characterization*, 3rd ed., p. 138, Wiley-Interscience, Hoboken, NJ (2006).
15. L. P. Floyd, T. Scheuermann, P. A. F. Herbert, and W. M. Kelly, *Solid-State Electron.*, **37**, 1579 (1994).
16. G. K. Reeves and H. B. Harrison, *IEEE Electron Device Lett.*, **3**, 111 (1982).
17. N. Lundberg and M. Östling, *Solid-State Electron.*, **38**, 2023 (1995).
18. C. N. Liao and T. H. She, *Thin Solid Films*, **515**, 8059 (2007).
19. C. N. Liao and S. W. Kuo, *J. Vac. Sci. Technol. A*, **23**, 559 (2005).
20. H. J. Ueng and D. B. Janes, *IEEE Trans. Electron Devices*, **48**, 758 (2001).
21. R. P. Gupta, O. D. Iyore, K. Xiong, J. B. White, K. Cho, H. N. Alshareef, and B. E. Gnade, *Electrochem. Solid-State Lett.*, **12**, H395 (2009).
22. O. D. Iyore, T. H. Lee, R. P. Gupta, J. B. White, H. N. Alshareef, M. J. Kim, and B. E. Gnade, *Surf. Interface Anal.*, **41**, 440 (2009).
23. K. Xiong, W. Wang, H. N. Alshareef, R. P. Gupta, J. B. White, B. E. Gnade, and K. Cho, *J. Phys. D: Appl. Phys.*, **43**, 115303 (2010).